PHYSICAL REVIEW C **69**, 034604 (2004)

Analysis of polarized $^{16}O(\vec{e},e'\vec{p})$ observables within the relativistic distorted wave impulse approximation

M. C. Martínez,[1] J. R. Vignote,[2] J. A. Caballero,[1] T. W. Donnelly,[3] E. Moya de Guerra,[4] and J. M. Udías[2]
[1]*Departamento de Física Atómica, Molecular y Nuclear, Universidad de Sevilla, Apartado Postal 1065, E-41080 Sevilla, Spain*
[2]*Departamento de Física Atómica, Molecular y Nuclear, Universidad Complutense de Madrid, E-28040 Madrid, Spain*
[3]*Center for Theoretical Physics, Laboratory for Nuclear Science and Department of Physics, Massachusetts Institute of Technology, Cambridge, Massachusetts 02139, USA*
[4]*Instituto de Estructura de la Materia, CSIC, Serrano 123, E-28006 Madrid, Spain*
(Received 22 September 2003; published 12 March 2004)

Recoil nucleon transferred polarization observables in coincidence quasielastic electron scattering are studied within the relativistic distorted wave impulse approximation. Results for response functions and polarization asymmetries are discussed for proton knockout from $p_{1/2}$, $p_{3/2}$, and $s_{1/2}$ shells in ^{16}O. The impact of spinor distortion is examined by comparing the fully relativistic calculation with results obtained by projecting out the negative-energy components. In particular, a careful analysis of effects linked to the description of the bound and scattered relativistic nucleon wave functions is presented. The high sensitivity of some polarization observables to the dynamical enhancement of the lower components, already shown within the relativistic plane wave impulse approximation, is proven to be maintained in the relativistic distorted wave approach. Semirelativistic approaches based on the effective momentum approximation are also studied. Finally, comparison with experimental data and a brief analysis of effects linked to medium modified form factors is presented.

DOI: 10.1103/PhysRevC.69.034604 PACS number(s): 25.30.Rw, 14.20.Gk, 24.10.Jv, 24.30.Gd

I. INTRODUCTION

A very topical issue in nuclear physics at present is the search for evidence of possible modification of the nucleon form factors inside the nuclear medium. A number of double polarized $(\vec{e},e'\vec{p})$ experiments have been proposed or carried out recently to measure polarization transfer asymmetries, motivated by the hope that such observables may provide valuable information that can shed some light on this issue. Importantly, transferred polarization observables have been identified as being ideally suited for such studies: they are believed to be the least sensitive to most standard nuclear structure uncertainties and accordingly to provide the best opportunities for studying the nucleon form factors in the nuclear medium. Polarization transfer data have been reported recently for the case of $^{16}O(\vec{e},e'\vec{p})^{15}N$ in Ref. [1] and for $^4He(\vec{e},e'\vec{p})^3H$ in Refs. [2,3]. Although the experimental uncertainties in both cases make it difficult to draw unambiguous conclusions on the nucleon form factors inside the nuclei, the data in Ref. [3] do seem to favor such a possibility. Specifically, this means that comparisons of measured polarization asymmetries with those computed using the best currently available nuclear models for the states and operators involved in the coincidence reaction in fact show disagreements, and that these can be removed by modifying the nucleon form factors in a reasonable way.

Of course, what constitutes the "best currently available nuclear models" must be judged carefully. In particular, the kinematic regime where the measurements have been undertaken is at relatively high energy—to make the reaction sufficiently impulsive to be at all interpreted as a simple single-nucleon knockout reaction—and it is clear that relativistic effects in wave functions and operators are essential. So, for instance, the data in Ref. [2] disagree significantly with the standard nonrelativistic calculations; however, this cannot be taken as evidence for nucleon modifications, since one finds that the results are (not unexpectedly) much more in accord with a fully relativistic approach. Also recent data on induced polarization in ^{12}C [4] strongly support an analysis based on the fully relativistic formalism [5]. These results are not surprising since spin and relativity are intrinsically related, and hence one may *a priori* consider the relativistic formalism to be better suited to describe polarization observables.

Indeed, most electron scattering experiments performed in the last decade have involved energies and momenta high enough to invalidate the nonrelativistic approximations assumed within the standard nonrelativistic distorted wave impulse approximation (DWIA), i.e., bound and scattered wave functions given as solutions of the Schrödinger equation, and one-body current operator resulting from a nonrelativistic reduction. In the relativistic distorted wave impulse approximation (RDWIA), nucleon wave functions are described by solutions of the Dirac equation with scalar and vector $(S$-$V)$ potentials, and the relativistic free nucleon current operator is used.

Relativistic effects can be classified into two basic categories according to their origin, namely, kinematical and dynamical effects. The former are due to the truncation of the current operator within the nonrelativistic approach, the latter, dynamical effects, come from the difference between the relativistic and nonrelativistic wave functions. Here one may distinguish a dynamical depression of the upper component of the scattered nucleon wave function in the nuclear interior (Darwin term) and a dynamical enhancement of the lower components, mainly that corresponding to the bound nucleon wave function.

So far, RDWIA calculations for cross sections and re-

sponse functions at low and high missing momenta [6–10] have clearly improved the comparison with experimental data over the previous nonrelativistic approaches. Moreover, RDWIA also predicts larger spectroscopic factors which are more in accord with theoretical calculations which incorporate correlations [6,10].

Concerning the current operators, in some recent studies [11–15] new so-called "semirelativistic" approaches have been introduced to describe $(e,e'p)$ reactions. Here the semirelativistic current operators are obtained by expanding only in missing momentum over the nucleon mass while treating the transferred energy and momentum exactly. This new approach has been proven to retain important aspects of relativity, and hence its predictions, compared with the standard DWIA, agree much better with the RDWIA calculations.

Concerning dynamical effects, the enhancement of the lower components of bound Dirac spinors [9,10] (not present in the semirelativistic approaches) has been shown to play a crucial role in the description of the interference R^{TL} response and left-right asymmetry A_{TL}. Meson exchange currents and the Δ-isobar contribution have recently been analyzed in Refs. [16,17] within the semirelativistic approach, also showing very significant effects, particularly due to Δ, at large missing momentum $p \geqslant 300$ MeV/c.

In this paper we focus on the analysis of polarized A$(\vec{e},e'\vec{p})$B observables within the framework of the RDWIA. Our aim is to study the role played by both kinematical and dynamical relativistic effects in a consistent description of the polarized responses and asymmetries. This work extends the previous analyses presented in Refs. [18,19] within the plane wave approach, now including a realistic description of the final-state interactions (FSI) through relativistic optical potentials. The magnitude of relativistic effects on various transfer polarization observables is carefully examined, disentangling the role played by the various ingredients that enter in the fully relativistic formalism. In particular, we extend the study of Ref. [18] where within relativistic plane wave impulse approximation (RPWIA) we demonstrated the importance of the negative-energy components of the relativistic bound nucleon in the description of the polarized responses and transferred polarization asymmetries. The RDWIA analysis performed here allows one to examine also the dynamical enhancement of the lower components in the scattered Dirac wave functions and moreover, makes it possible to carry out meaningful comparisons with measured observables.

Returning to the issue of potential medium modifications of the nucleon form factors, the current study has the following goal: we wish to explore a selected set of model "variations on a theme" of the type discussed above. In all cases we choose only modeling, that is, within the context of the general relativistic approach being adopted, consistent with what we know about initial- and final-state wave functions and one-body electromagnetic operators. Since equally acceptable relativistic potentials exist when obtaining the states and since alternative descriptions of the current operators are likewise acceptable, it is impossible at present to define what is "the best" model. Our goal is to explore these acceptable models and where the resulting polarization observables differ with the choice of model to ascribe these variations to a (minimal) theoretical uncertainty. Needless to say, all of this is within the general context of relativistic mean-field modeling and so the resulting uncertainties are minimal in the sense that effects that go beyond the scope of the modeling might increase the uncertainties. In the final analysis, only if medium modification effects are larger than the uncertainties we find here, and only if the uncertainties that arise from ingredients not in the present model can ultimately be shown to be small, will a convincing case be made for the necessity of having such medium modification effects.

The paper is organized as follows. In Sec. II we briefly introduce the general formalism for A$(\vec{e},e'\vec{p})$B reactions focusing on the relativistic distorted wave impulse approximation. Within this context, we also introduce the projected approach, the effective momentum approximation (EMA-noSV) and the use of semirelativistic current operators. By comparing them one may get a clear image of the importance of relativity in these processes. In Sec. III we present and discuss the results, paying special attention to the polarized responses and transferred polarization asymmetries. Finally, in Sec. IV we summarize our conclusions.

II. DESCRIPTION OF $A(\vec{e},e'\vec{p})B$ REACTIONS

A. General formalism: RDWIA

In this section we briefly review the general formalism needed to describe coincidence $(\vec{e},e'\vec{p})$ reactions. We consider plane waves for the incoming and outgoing electron (treated in the extreme relativistic limit) and the Born approximation (one virtual photon exchanged). When the incoming electron is polarized and the final nucleon polarization is measured, the differential cross section can be written as [20–24]

$$\frac{d\sigma}{d\varepsilon_e d\Omega_e d\Omega_F} = \frac{\sigma_0}{2}[1 + \mathbf{P}\cdot\boldsymbol{\sigma} + h(A + \mathbf{P}'\cdot\boldsymbol{\sigma})], \qquad (1)$$

where the variables $\{\varepsilon_e,\Omega_e\}$ refer to the scattered electron and Ω_F to the ejected nucleon. The term σ_0 is the unpolarized cross section, h is the incident electron helicity, A denotes the electron analyzing power, and $\mathbf{P}(\mathbf{P}')$ represents the induced (transferred) polarization. Note that both $\mathbf{P}$ and $\mathbf{P}'$ depend on the outgoing nucleon polarization, but $\mathbf{P}'$ only becomes accessible when the incoming electron beam is polarized. The cross section in Eq. (1) can also be written in terms of nuclear responses as follows:

$$\begin{aligned}\frac{d\sigma}{d\varepsilon_e d\Omega_e d\Omega_F} = K\sigma_M f_{rec}^{-1}\{&v_L(R^L + R_n^L\hat{S}_n) + v_T(R^T + R_n^T\hat{S}_n)\\ &+ v_{TL}[(R^{TL} + R_n^{TL}\hat{S}_n)\cos\phi + (R_l^{TL}\hat{S}_l\\ &+ R_s^{TL}\hat{S}_s)\sin\phi] + v_{TT}[(R^{TT} + R_n^{TT}\hat{S}_n)\cos 2\phi\\ &+ (R_l^{TT}\hat{S}_l + R_s^{TT}\hat{S}_s)\sin 2\phi] + h\{v_{TL'}[(R_l^{TL'}\hat{S}_l\\ &+ R_s^{TL'}\hat{S}_s)\cos\phi + (R^{TL'} + R_n^{TL'}\hat{S}_n)\sin\phi]\\ &+ v_{T'}[R_l^{T'}\hat{S}_l + R_s^{T'}\hat{S}_s]\}\},\end{aligned} \qquad (2)$$

where ϕ is the azimuthal angle that determines the outgoing

nucleon momentum. The term K is a kinematical factor given by $K=p_F M_N M_B/M_A$, with p_F the outgoing nucleon momentum, M_N the nucleon mass, and $M_B(M_A)$ the mass of the residual nucleus (target), respectively. The Mott cross section is represented by σ_M, f_{rec} is the recoil factor given by $f_{rec}=1+(\omega p_F - qE_F \cos\theta_F)/M_A p_F$, where E_F is the outgoing nucleon energy and θ_F is the angle between $\mathbf{p}_F$ and the transferred momentum, and the v_K, $K=L$, T, … are the standard electron scattering kinematical factors (see Refs. [24,25]). The indices l, s, n refer as usual to the directions selected to specify the recoil nucleon polarization: **l** (parallel to the momentum $\mathbf{p}_F$), **n** (perpendicular to the plane containing $\mathbf{p}_F$ and the transfer momentum **q**), and **s** (determined by $\mathbf{n}\times\mathbf{l}$). From this large number of possible response functions some selection can be made to limit the focus: (i) Assuming coplanar kinematics, i.e., $\phi=0°,180°$, from the total set of 18 responses in Eq. (2) only 12 survive. (ii) From these twelve responses, the four transferred polarization ones $R_{l,s}^{K'}$ only contribute when the electron is polarized, while the four induced polarization ones R_n^K only enter when FSI are taken into account.

Following the analysis presented in Ref. [18], in this work we limit our attention to those observables that survive in the plane wave limit, i.e., transferred polarization responses $R_l^{TL'}$, $R_l^{T'}$, $R_s^{TL'}$, $R_s^{T'}$ and transferred asymmetries P_l', P_s'. A detailed study of the induced polarization observables within RDWIA has been presented in Ref. [5].

The response functions in Eq. (2) are constructed directly by taking the appropriate components of the hadronic tensor $W^{\mu\nu}$ which, within the RDWIA, comes from bilinear combinations of the nucleon current matrix elements

$$J_N^\mu(\omega,\mathbf{q}) = \int d\mathbf{p}\,\overline{\Psi}_F(\mathbf{p}+\mathbf{q})\hat{J}_N^\mu \Psi_B(\mathbf{p}), \tag{3}$$

where Ψ_B and Ψ_F are relativistic wave functions describing the initial bound and final outgoing nucleons, respectively, and $\hat{J}_N^\mu$ is the relativistic one-body current operator. The bound wave function Ψ_B is a four-spinor with well-defined parity and angular momentum quantum numbers κ_b, μ_b, obtained within the framework of the relativistic independent particle shell model. The mean field in the Dirac equation is determined through a Hartree procedure from a phenomenological relativistic Lagrangian with scalar (S) and vector (V) terms. It may be written

$$\Psi_B(\mathbf{p}) = \Psi_{\kappa_b}^{\mu_b}(\mathbf{p}) = \frac{1}{(2\pi)^{3/2}}\int d\mathbf{r} e^{-i\mathbf{p}\cdot\mathbf{r}}\Psi_{\kappa_b}^{\mu_b}(\mathbf{r}) = (-i)^{\ell_b}\begin{pmatrix} g_{\kappa_b}(p) \\ S_{\kappa_b} f_{\kappa_b}(p)\dfrac{\boldsymbol{\sigma}\cdot\mathbf{p}}{p}\end{pmatrix}\Phi_{\kappa_b}^{\mu_b}(\hat{\mathbf{p}}) \tag{4}$$

with $\Phi_{\kappa_b}^{\mu_b}(\hat{\mathbf{p}})$ the usual spinor harmonics. The wave function for the ejected proton Ψ_F is a scattering solution of a Dirac-like equation, which includes S-V global optical potentials obtained by fitting elastic proton scattering data. This wave function, obtained as a partial wave expansion, is given in momentum space by

$$\Psi_F(\mathbf{p}) = 4\pi\sqrt{\frac{E_F+M_N}{2E_F}} \times \sum_{\kappa\mu m} e^{-i\delta_\kappa^*} i^\ell \langle \ell m \tfrac{1}{2} s_F | j\mu\rangle Y_\ell^{m*}(\hat{\mathbf{p}}_F)\Psi_\kappa^\mu(\mathbf{p}), \tag{5}$$

where $\Psi_\kappa^\mu(\mathbf{p})$ are four-spinors of the same form as in Eq. (4), but the phase shifts and radial functions are complex because of the complex optical potential involved.

Finally, for the nucleon current operator we consider the two choices denoted as CC1 and CC2 [26]

$$\hat{J}_{CC1}^\mu = (F_1+F_2)\gamma^\mu - \frac{F_2}{2M_N}(\overline{P}+P_F)^\mu, \tag{6}$$

$$\hat{J}_{CC2}^\mu = F_1\gamma^\mu + i\frac{F_2}{2M_N}\sigma^{\mu\nu}Q_\nu, \tag{7}$$

where F_1 and F_2 are the Dirac and Pauli nucleon form factors related to the electric and magnetic Sachs form factors in the usual form. The variable $\overline{P^\mu}$ in Eq. (6) is the four-momentum of the initial nucleon for on-shell kinematics, i.e., $\overline{P^\mu}=(\overline{E},\mathbf{p})$ ($\overline{E}=\sqrt{\mathbf{p}^2+M_N^2}$ and $\mathbf{p}=\mathbf{p}_F-\mathbf{q}$).

B. Dynamical effects: projected approach and effective momentum approximation

In recent years a considerable effort has been devoted to the analysis of quasielastic $(e,e'p)$ reactions using a fully relativistic formalism. Within this framework, particular emphasis has been placed on comparison between relativistic and nonrelativistic approaches, trying to identify and disentangle clearly the ingredients which lead to different results in the two types of calculations. In some recent works [27], relativistic effects have been analyzed by comparing directly results obtained from a standard nonrelativistic DWIA code (DWEEPY) with those provided by a relativistic calculation. These investigations were aimed at providing systematic and precise information on the magnitude of the effects introduced by relativity when compared with the standard nonrelativistic description based on DWEEPY. The latter was widely used in the 1980's to analyze low-energy experimental data. However, although interesting, this study did not allow one to identify clearly the role played by the various ingredients entering into the relativistic formalism. Note that apart from the four-spinor versus two-spinor structure involved in relativistic and nonrelativistic calculations, respectively, also the potentials used in the Dirac and Schrödinger equations for the bound and scattered nucleon are different. Moreover, the nonrelativistic current operator results from an expansion in a basis of free nucleon plane waves and a Pauli reduction with the operator expanded in powers of p/M_N, q/M_N, and/or ω/M_N, p being the missing momentum, q and ω the transfer momentum and energy, respectively. In this work we focus on the separate analysis of the various ingredients that enter in the general formalism, and evaluate their impact on the transferred polarization observables. Hence, in order to minimize the mismatch coming from the different assumptions involved in relativistic and nonrelativistic approaches,

all of the results presented in this work have been evaluated using the same potentials and code.

Dynamical effects arise from the differences between relativistic and nonrelativistic potentials and wave functions. A detailed study on this subject has been already presented in Refs. [9,10,28], so here we simply summarize the basic concepts needed for later discussion of the results. As is well known, interacting Dirac wave functions have a nonzero overlap with the Dirac sea [29]. The presence of the *S*-*V* potentials leads to a significant dynamical enhancement of the lower components of the Dirac solution at the nuclear interior. This fact is clearly illustrated by realizing that for a general solution of the Dirac equation with scalar and vector potentials, its upper and lower components are related by

$$\Psi^{down} = \frac{\boldsymbol{\sigma}\cdot\mathbf{p}}{E + M_N + S - V}\Psi^{up} \tag{8}$$

with $S<0$ and $V>0$. Note that these lower components are enhanced with respect to the ones corresponding to free positive energy spinors where $S=V=0$. This effect has been referred to as dynamical enhancement of the lower components, and more recently as *spinor distortion* [30].

The analysis of these dynamical effects can be done by constructing properly normalized four-spinor wave functions where the negative-energy components have been projected out. Thus, instead of the fully relativistic expression given in Eq. (3), the nucleon current is evaluated as

$$J_N^{\mu(+,+)}(\omega,\mathbf{q}) = \int d\mathbf{p}\,\overline{\Psi}_F^{(+)}(\mathbf{p}+\mathbf{q})\hat{J}_N^{\mu}\Psi_B^{(+)}(\mathbf{p}), \tag{9}$$

where $\Psi_B^{(+)}(\mathbf{p})$, $[\Psi_F^{(+)}(\mathbf{p})]$ is the positive-energy projection of $\Psi_B(\mathbf{p})$, $[\Psi_F(\mathbf{p})]$, i.e.,

$$\Psi_B^{(+)}(\mathbf{p}) = \Lambda_{(+)}(\mathbf{p})\Psi_B(\mathbf{p})$$

$$\Psi_F^{(+)}(\mathbf{p}+\mathbf{q}) = \Lambda_{(+)}(\mathbf{p}+\mathbf{q})\Psi_F(\mathbf{p}+\mathbf{q}), \tag{10}$$

where $\Lambda_{(+)}(\mathbf{p})=(M_N+\overline{P})/2M_N$ is the positive-energy projector. Then the effects due to the dynamical enhancement of the lower components show up clearly by comparing the results obtained using the fully relativistic amplitude given in Eq. (3) with those evaluated by using Eq. (9).

Note that the relationship between lower and upper components in the projected wave functions is similar to that corresponding to free nucleon wave functions, but with the positive-energy projectors depending explicitly on the integration variable **p**. An additional approach, referred to as asymptotic projection, consists of introducing the asymptotic values of the momenta into the positive-energy projectors acting on the bound and scattered wave functions. This asymptotic projection is very similar (although it is not completely equivalent) to the EMA-noSV introduced originally by Kelly [30]. Within the EMA-noSV approach, the four spinors used have the same upper components as those of the Dirac equation solutions, but the lower components are obtained by enforcing the "free" relationship between upper and lower components and using the asymptotic momenta at the nucleon vertex. Note that these wave functions also lack the dynamical enhancement of the lower components.

Finally, one also has the dynamical quenching of the upper component of the Dirac wave function in the nuclear interior compared with the nonrelativistic solution. This effect, associated with the Darwin term, is implicitly included in all calculations presented in this work. Hence the differences between the EMA-noSV approach (or equivalently the asymptotic projection) and the fully relativistic calculation can be solely ascribed to the negative-energy components.

C. Kinematical effects: semi-relativistic reductions

Another ingredient which leads to differences between the relativistic and nonrelativistic approaches concerns the specific form of the current operator used to evaluate Eq. (3). Instead of the fully relativistic operator considered in RDWIA, truncated expressions up to first or higher orders in p/M_N, ω/M_N, and/or q/M_N are employed in standard nonrelativistic DWIA calculations. These effects, here referred to as kinematical relativistic effects [9,10,19], include not only the relativistic kinematics of the nucleon energies and momenta [16,31] (which must be accounted for in order to describe properly the form of the momentum distribution), but also the effects linked to the use of the relativistic nucleon current operator.

Improved nonrelativistic expansions of the nucleon current operator, denoted as semirelativistic approaches, which contain important aspects of relativity, have been derived recently and are available in the literature [12–15]. In this paper we investigate the kinematical effects associated with these expansions in polarized $(\vec{e},e'\vec{p})$ observables. To this end we have also incorporated the semirelativistic expressions in the relativistic code, so that a direct comparison between the fully relativistic calculation and the semirelativistic approach becomes more meaningful because the effects due to the choice of wave functions and/or potentials are minimized.

To make the analysis clearer, in what follows we explain in some detail the procedure used to get the semirelativistic results. In the case in which spinor distortion is neglected and asymptotic momenta are used, the relativistic (4×4) current matrix element can be recast in an equivalent form that involves an effective (2×2) current operator $\overline{J}^{\mu}_{eff}$ that occurs between the upper two component spin $\frac{1}{2}$ spinors. The (2×2) operator $\overline{J}^{\mu}_{eff}$ is obtained without any approximation concerning nonrelativistic reductions; it corresponds to an exact expression for the on-shell electromagnetic current operator [15]. This means that the results obtained using $\overline{J}^{\mu}_{eff}$ between bispinors corresponding to the upper components of the relativistic wave functions should coincide exactly with those obtained using the original relativistic (4×4) electromagnetic current operator within the EMA-noSV approach

[30]. Finally, a comparison between these results and those provided by making use of the semirelativistic expressions for the operator, leads to direct information on the magnitude associated with the kinematical relativistic effects. It is important to point out that the semirelativistic reduction is done in the context of the effective momentum approximation, i.e., using asymptotic momenta.

The semirelativistic expression of the electromagnetic current operator relies on the direct Pauli reduction method, by expanding only in the missing momentum (p) over the nucleon mass. The transfer energy and momentum are treated exactly. Up to first-order in p/M_N, the following results for the electromagnetic current operators are obtained:

$$\bar{J}^0 = \frac{\kappa}{\sqrt{\tau}} G_E + \frac{i}{\sqrt{1+\tau}} \left(G_M - \frac{G_E}{2} \right) (\boldsymbol{\kappa} \times \boldsymbol{\eta}) \cdot \boldsymbol{\sigma}, \tag{11}$$

$$\begin{aligned} \bar{\mathbf{J}} = \frac{1}{\sqrt{1+\tau}} \Bigg\{ & i G_M (\boldsymbol{\sigma} \times \boldsymbol{\kappa}) + \left(G_E + \frac{\tau}{2} G_M \right) \boldsymbol{\eta} + G_E \boldsymbol{\kappa} \\ & - \frac{G_M}{2(1+\tau)} (\boldsymbol{\kappa} \cdot \boldsymbol{\eta}) \boldsymbol{\kappa} - \frac{i G_E}{2(1+\tau)} (\boldsymbol{\sigma} \times \boldsymbol{\kappa}) \boldsymbol{\kappa} \cdot \boldsymbol{\eta} - i\tau \\ & \times \left(G_M - \frac{G_E}{2} \right) (\boldsymbol{\sigma} \times \boldsymbol{\eta}) + \frac{i(G_M - G_E)}{2(1+\tau)} (\boldsymbol{\kappa} \times \boldsymbol{\eta}) \boldsymbol{\sigma} \cdot \boldsymbol{\kappa} \Bigg\}, \end{aligned} \tag{12}$$

where we have introduced the usual dimensionless variables: $\tau = |Q^2|/4M_N^2$, $\boldsymbol{\kappa} = \mathbf{q}/2M_N$ and $\boldsymbol{\eta} = \mathbf{p}/M_N$. Obviously, when computing response functions, evaluated by taking bilinear combinations of the electromagnetic current matrix elements, terms of order η^2 should be dismissed.

As shown, the spin-orbit part of the charge and the relativistic correction to the transverse current, the first-order convective spin-orbit term, are included in Eqs. (11) and (12). Although the above expressions have been already presented in the literature [12–15,31], in most of these previous works the analysis of the observables has been performed adopting additional approximations on the vector current, namely, $\bar{\mathbf{J}}$ is simply taken as the standard nonrelativistic reduction except for a global kinematical factor $(1+\tau)^{-1/2}$ that includes relativistic corrections coming from the Dirac spinors (see Refs. [12–15] for details). Here we evaluate the recoil nucleon polarized observables by making use of the full semirelativistic currents in Eqs. (11) and (12) taken between the upper components of the original relativistic wave functions.

III. RESULTS AND DISCUSSION

In this section we analyze the recoil nucleon transferred polarization observables for proton knockout from ^{16}O. Although we focus on results for the $1p_{1/2}$ shell, similar conclusions are reached for the $1p_{3/2}$ and $1s_{1/2}$ shells unless otherwise specified. Results are computed for both CC1 and CC2 choices of the current operator in Eqs. (6) and (7), and the Coulomb gauge is assumed. A detailed study on gauge ambiguities in RPWIA has been presented in Ref. [18] showing that the Coulomb and Landau gauges lead to very similar results, differing significantly from the ones corresponding to the Weyl gauge. These results are proven to persist within the relativistic distorted approach. The bound nucleon wave function is obtained using the parameters of the set NLSH [32]. Results computed with other parameterizations are found to be similar and do not change the general conclusions. For the outgoing nucleon wave function, we use the energy-dependent, A-independent potential derived by Clark *et al.* for ^{16}O (EDAIO) [33] which describes fairly well the existing elastic proton-^{16}O scattering data. Although our main interest in this work concerns the effects introduced by dynamical and kinematical relativistic effects, a brief study of the sensitivity of the polarized observables to the description of final-state interactions is also presented. Hence in following section, results evaluated with different relativistic optical potentials are shown and compared. Finally, the Coulomb distortion of the electron wave functions is accounted for by using the effective momentum approximation with the nuclear Coulomb potential equal to 3.5 MeV (see Refs. [6,7] for details). All the results shown throughout this work correspond to the nucleon form factor parametrization of Gari and Krumplemann [34].

A. Final-State Interactions: relativistic optical potentials

We start our discussion with the analysis of the longitudinal and sideways transferred polarization asymmetries and their dependence on FSI. In Fig. 1, P_l' and P_s' are presented as functions of the missing momentum p. The kinematics are chosen with (q,ω) constant, $q=1$ GeV/c and $\omega=439$ MeV, yielding $|Q^2|=0.8$ (GeV/c)^2. This roughly corresponds to the experimental conditions of experiments E89-003 and E89-033 performed at JLab [35–37]. Left panels correspond to the $p_{1/2}$ shell and right panels to $p_{3/2}$. In each case, RDWIA results obtained with the EDAIO optical potential parametrization [33] are compared with the RPWIA results. Plane wave calculations after projecting out the negative-energy components of the bound nucleon wave function, denoted as PWIA, are also shown. Note that PWIA polarization transfer asymmetries coincides with what one would obtain using free Dirac spinors wave functions for both nucleons in Eq. (3). The electron beam energy has been fixed to $\varepsilon_{beam}=2.445$ GeV which corresponds to an electron scattering angle $\theta_e=23.4°$ (forward scattering).

First note the difference between the RPWIA calculations (dot-dashed lines) and the RDWIA results (solid lines). For low missing momentum values $p \lesssim 200$ MeV/c, the effects of FSI do not modify substantially the behavior of the polarization asymmetries, particularly for P_l'. However, in the case of P_s', the difference is of the order of 20–25% for $p \simeq 100$ MeV/c which corresponds to the momentum where the responses reach their maxima for the $p_{1/2}$ shell. Similar comments also apply to the results obtained for the $p_{3/2}$ and $s_{1/2}$ shells, although in these cases a smaller effect of FSI is observed for P_s'. It is important to point out that FSI lead to a significant reduction of the individual response functions: ~50–60% ($R_l^{TL'}$) and ~25% ($R_s^{TL'}$ and $R_l^{T'}$) at $p \simeq 100$ MeV/c. The response $R_s^{T'}$ is very small and its contribution to the transferred polarization is hardly visible.

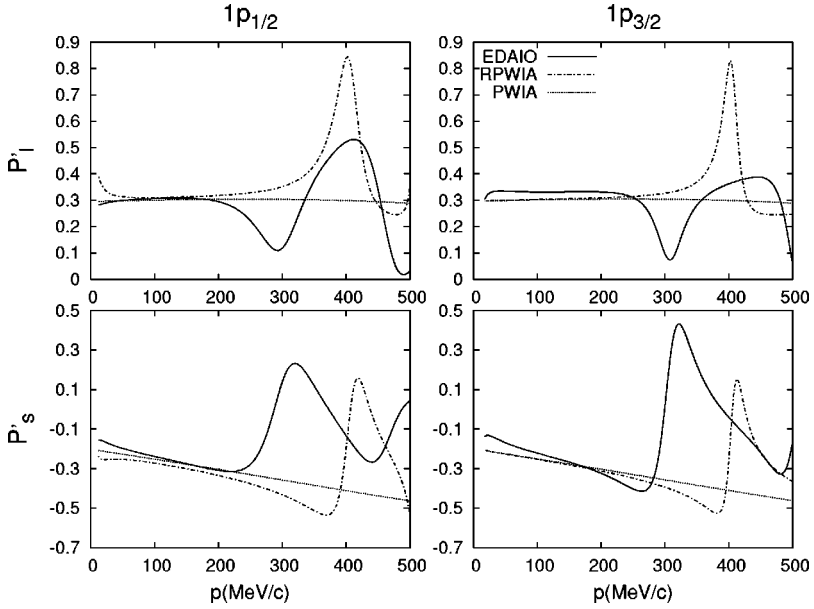

FIG. 1. Transferred polarization asymmetries for the $p_{1/2}$ (left panels) and $p_{3/2}$ (right panels) shells in (q,ω)-constant kinematics (see text). Top and bottom panels correspond to the longitudinal and sideways components, respectively. RPWIA results (dot-dashed lines) are compared with RDWIA calculations using EDAIO (solid lines), and with the PWIA (dotted line) (see text for details). All calculations correspond to the CC2 current operator.

Hence, the results in Fig. 1 clearly indicate that for low p values, FSI effects are partially canceled when constructing the transferred polarization asymmetries. Note also that, for these low-p values, the PWIA approach is more in accord with the RDWIA. This means that in RPWIA the role of dynamical relativity stands out more clearly.

For high missing momentum, $p \gtrsim 200\ \mathrm{MeV}/c$, FSI strongly modify the behavior of the polarizations, which is in accord with the peculiar sensitivity to the interaction presented by each response function. When comparing RDWIA with RPWIA we see that the main effect is a global displacement to lower momenta of the polarization profiles. Let us recall that the oscillatory behavior shown by P_l' and P_s' within RPWIA is a direct consequence of the dynamical enhancement of the lower components in the bound Dirac wave functions [18]; thus disappearing within PWIA. The oscillations are also present in the relativistic distorted wave calculations, although being very different from the RPWIA results with the maxima and minima located at different p values. Let us note that the oscillatory behavior of the polarization asymmetries persists even when nonrelativistic distorted wave approaches are assumed (see Refs. [17,27,38]). This outcome emerges due to the fact that both FSI and dynamical relativistic effects cause a breakdown of factorization. A study of the latter is presently in progress and the results will be presented in a forthcoming publication [39].

Let us next focus on the analysis of the uncertainties introduced by different relativistic optical potentials. In Fig. 2 we present the transferred ratios P_l' and P_s' for the $p_{1/2}$ shell evaluated using three different relativistic optical potential parametrizations: EDAIO, EDAD1, and EDAD2 [33]. Results with EDAD3 parameterization are practically identical to those obtained with EDAD1 and therefore have not been plotted. The left panels refer to calculations involving the CC1 current operator and right panels to CC2. As pointed out in previous papers [17,21,27,30], transferred polarization

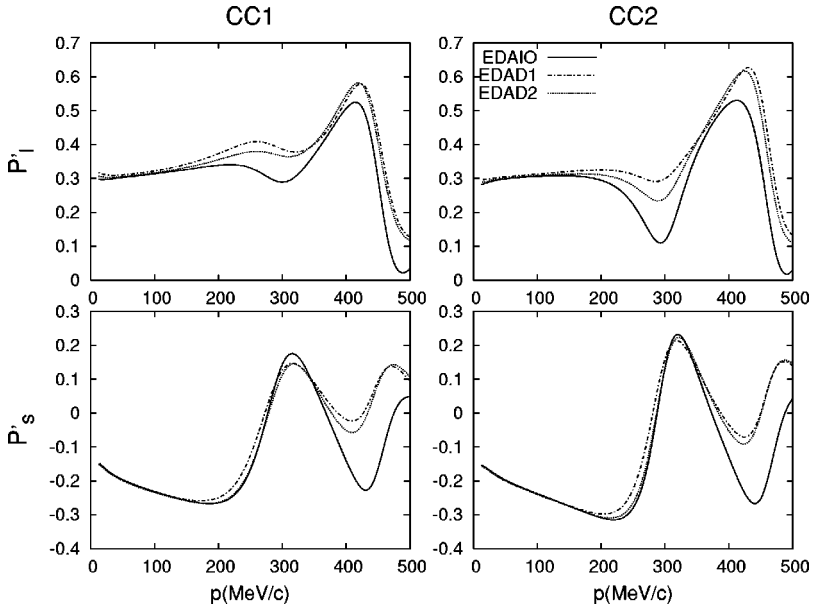

FIG. 2. Transferred polarization asymmetries for the $p_{1/2}$ shell in (q,ω)-constant kinematics. Top and bottom panels correspond to the longitudinal and sideways components, respectively. Right panels refer to results obtained with the CC2 current operator and left ones to the CC1 current. RDWIA calculations using EDAIO (solid lines), EDAD1 (dot-dashed lines) and EDAD2 (dotted lines) optical potential parameterizations are compared.

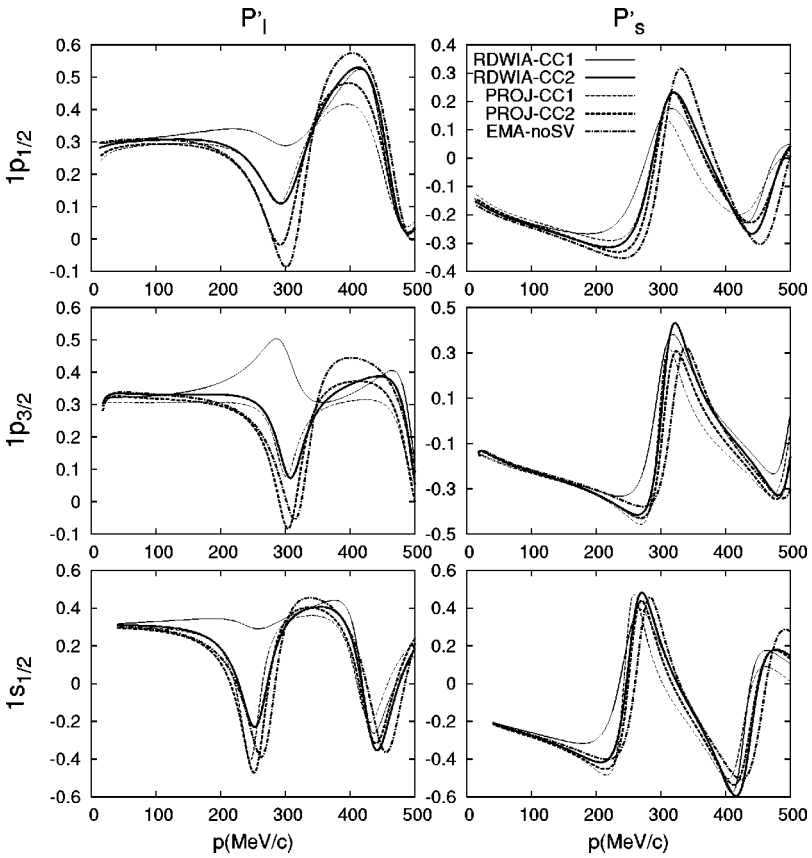

FIG. 3. Same observables as in Fig. 1. Right panels correspond to P'_s and left ones to P'_l. On top, middle, and bottom panels, results for the $1p_{1/2}$, $1p_{3/2}$, and $1s_{1/2}$ shells are plotted, respectively. In each graph, RDWIA calculations evaluated with EDAIO (solid line) are compared with positive-energy projection results (dashed line) and EMA-noSV approach (dot-dashed line). Thick lines correspond to the CC2 current operator and thin lines to CC1.

asymmetries are expected to be relatively insensitive to the choice of optical potential at low missing momenta. This can be seen in Fig. 2, at least up to $p=150$ MeV/c which is where the cross section reaches its maximum value [37]. This trend is also followed in the other two shells, $p_{3/2}$ and $s_{1/2}$.

However, as shown in Fig. 2, P'_l exhibits a strong dependence on the optical potential parametrization, resulting in important differences for larger values of the missing momentum: ~20% (CC1) and ~40% (CC2) for $p \simeq 250$ MeV/c. Note that in this kinematical region the cross section [37] has already decreased by almost two orders of magnitude with regards to the maximum, making measurements of transferred polarization responses very difficult. This result contrasts with nonrelativistic and semirelativistic approaches where the effects introduced by different nonrelativistic optical potentials are small [17]. Note also that the current operator choice, CC1 versus CC2, gives rise to very significant differences in P'_l within this p region, being of the same order as those introduced by the optical potentials. Only for high p values, $p \gtrsim 350$ MeV/c, is the uncertainty associated with FSI larger than that due to the choice of current operator. In the case of the sideways polarization P'_s, in general less dependence on the interaction model as well as on the current is seen, which is more in accord with nonrelativistic analyses. Finally, note that for very high momentum values $p \gtrsim 400$ MeV/c, P'_l and P'_s evaluated with the EDAIO potential deviate from the results corresponding to the EDAD1 and EDAD2 parameterizations.

To end with this discussion, we conclude that both transferred polarization asymmetries at moderate p values ($p \simeq 100$ MeV/c) are independent of the optical potential choice. Increasing p from here, each optical potential starts to follow a different curve especially in the case of P'_l. For very high p ($p \gtrsim 350$ MeV/c), both transferred polarizations present large sensitivity to the choice of optical potential. However, caution should be placed on drawing general conclusions from the results given here in this kinematical region because other ingredients beyond the impulse approximation, such as meson exchange currents (MEC), Δ-isobar, short-range correlations, etc., may also play a crucial role.

B. Dynamical relativistic effects

This section, which constitutes the main focus of the present work, is devoted to the analysis of dynamical relativistic effects for nucleon polarized observables within the framework of the RDWIA. With this aim we present in Fig. 3 the longitudinal and sideways transferred polarization asymmetries for the three shells involved in ^{16}O: $p_{1/2}$, $p_{3/2}$, and $s_{1/2}$. All of the results have been obtained using the EDAIO optical potential parametrization [33], and the choice of kinematics is the same as in the previous figures. To make explicit the effects introduced by spinor distortion, in each graph we compare the fully relativistic calculations (solid lines) using both current operators, CC1 (thin lines) and CC2 (thick lines), with the results after projecting out the negative-energy components [see Eqs. (9) and (10)] (dashed lines). Finally we also present for reference the results corresponding to the EMA-noSV approach evaluated with the CC2 current operator (dot-dashed line). Within EMA-noSV,

the results provided by the two current operators are very similar, differing only due to the off-shell kinematical quantities involved in the operator [19,28].

A detailed analysis of the transferred polarizations within the relativistic plane wave approach was presented in Ref. [18]. In said reference, it is shown that the dynamical enhancement of the lower components in the bound nucleon wave function leads to strong oscillations in $P'_{l,s}$ for high missing momentum values, $p \geqslant 300$ MeV/c. This behavior disappears after projecting out the negative-energy components. From the results shown in Fig. 3, it is clear that, within the relativistic distorted wave approximation, the oscillatory behavior in the polarization asymmetries persists even after projecting the bound and scattered proton wave functions over positive-energy states. The same comment applies to the EMA-noSV approach. On the contrary, this last fact is not applicable to the behavior shown by the left-right asymmetry A_{TL} [9,10], defined as the difference of unpolarized cross sections evaluated at $\phi=0°$ and $\phi=180°$ divided by their sum. These results are connected with the interplay between polarization degrees of freedom and dynamical relativistic effects. Whereas in RPWIA, projecting out the negative-energy components of the bound nucleon wave function leads to factorization, hence destroying the oscillatory behavior in $P'_{l,s}$, in RDWIA factorization breaks down even after projection over positive-energy components.

From inspection of Fig. 3, and in accord with previous results for unpolarized observables [9,10,28] and polarized ones in RPWIA [18], we note that dynamical relativistic effects are maximized for the CC1 current operator. This applies to both polarization ratios and the three shells considered. Particularly noteworthy is the behavior displayed by P'_l even at intermediate p values in the case of the fully relativistic CC1 calculation. This result deviates significantly from the others, modifying even the global shape of the observable. This contrasts with the situation for P'_s where, apart from the specific discrepancies introduced by relativity, the five calculations follow the same general oscillatory pattern. Hence it would be interesting to investigate further this intermediate p region where new high quality data on P'_l could make it possible to constrain the theoretical choices for current operator.

As shown in Refs. [9,28], the contribution from the negative-energy components to the current are of the same order as the positive-energy ones with the CC2 operator, whereas with the CC1 choice the negative-energy terms may become much larger. This explains the much wider spread shown by the CC1 results, particularly the large effects introduced by the dynamical enhancement of the lower components in P'_l. As we will show later, this emerges from the polarized responses that enter in the longitudinal polarization in contrast with the sideways case. Note also that the CC1 projected calculations get closer to the CC2 ones and to the EMA-noSV approach. This may indicate that the CC1 current emphasizes the role played by the lower components in the wave functions, agreeing with the findings for unpolarized responses [10]. Precise comparisons with data would yield definite conclusions on the reliability of the various approximations.

Finally, it is also interesting to compare the effects arising from dynamical relativity with those due to FSI models. As shown in Figs. 1–3, P'_l presents the strongest sensitivity to both kinds of effects for intermediate p values, $200 \leqslant p \leqslant 350$ MeV/c. This can make it difficult to isolate the role played by each ingredient when compared with data; however, note that the important deviation between the results obtained with the two currents tends to persist, no matter which optical potential is used. Hence, precise measurements of P'_l in this p region, in conjunction with P'_s data, may give us important clues to constrain final-state interactions and the choice of current operator.

To complete the analysis of dynamical relativistic effects, we focus on the four separate responses that contribute when the polarization of the outgoing nucleon is measured and the electron beam is polarized: $R_l^{T'}$, $R_l^{TL'}$, $R_s^{T'}$, and $R_s^{TL'}$ ($R_n^{TL'}$ does not enter for coplanar kinematics). Results are shown in Fig. 4 for proton knockout in ^{16}O from the $p_{1/2}$ shell. Let us recall that Coulomb distortion of the electron waves breaks the simplicity of Eq. (2), leading to responses which also depend on the electron kinematic variables. However, the effective momentum approximation for the electrons adopted in this work makes Eq. (2) reliable when analyzing the response functions. For ^{16}O we have proven [10] that Coulomb distortion effects, and consequently the dependence of the responses with θ_e, are very small.

As a general rule we observe that $R_s^{T'}$ and $R_l^{TL'}$ show the highest sensitivity to relativistic dynamics, while the uncertainties in $R_l^{T'}$ and $R_s^{TL'}$ are much smaller. This coincides with the analysis already performed in RPWIA [18] and, although not shown here for simplicity, applies also to the $p_{3/2}$ and $s_{1/2}$ shells. In addition, Gordon ambiguities are also significantly enhanced for $R_s^{T'}$ and $R_l^{TL'}$. Finally, note that the largest spread due to relativistic dynamical effects arises for the CC1 current operator, which is in accord with RPWIA results [18], and can be traced back to the strong influence of the negative-energy projections of the wave functions in this case.

Let us study in more detail each individual response. As shown in Fig. 4, the contributions of $R_l^{T'}$ and $R_s^{TL'}$ are rather similar, and moreover, the EMA-noSV predictions almost coincide (evaluated at the maxima) with the fully relativistic calculations, the largest difference being of the order of 3.6% for the CC1 current in $R_s^{TL'}$. Positive-energy projected results also follow the RDWIA curves closely, although sizeable differences are observed for the CC1 current, particularly in the case of $R_l^{T'}$ (~11% at the maximum).

Concerning $R_l^{TL'}$, we observe that the projected calculations differ substantially from the RDWIA results, especially for the CC1 current operator. This resembles the large relativistic dynamical effects shown by this response in RPWIA [18]. On the contrary, it is interesting to note that different choices of the current operator within RDWIA lead to very similar results, which is somewhat opposed to the situation observed in the plane wave limit [18]. Finally, the EMA-noSV approach provides a description of $R_l^{TL'}$ that basically coincides with the two RDWIA calculations, the largest difference being observed at very low-p values. In fact, this result is proven to be valid only at $q=1$ GeV/c, where the effective momentum approach (EMA) applied to the bound

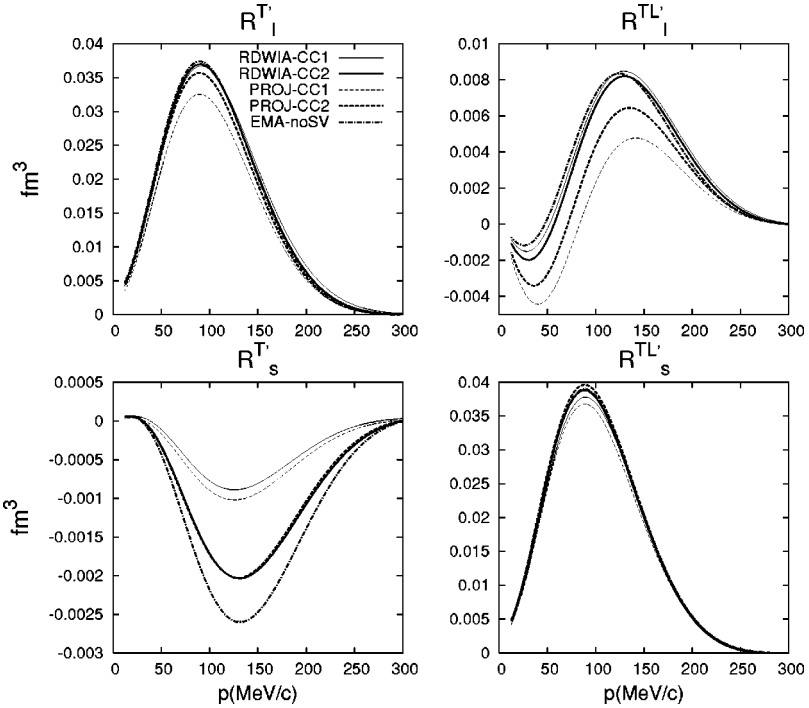

FIG. 4. Transferred polarized responses for the $1p_{1/2}$ shell. Same kinematics as in preceding figures, and the labeling as in Fig. 2.

wave function, leads to effects which cancel almost exactly those coming from the ejected nucleon. For lower values of q this cancellation does not occur, and so an important discrepancy between the EMA-noSV prediction and the RDWIA calculations emerges.

The smallest $R_s^{T'}$ response presents a large dependence on the current operator choice. This applies to the full RDWIA calculation as well as to the positive-energy projected approach. Note, however, that the difference between RDWIA and projected results is tiny, almost negligible for the CC2 current. Contrary to $R_l^{TL'}$ case, the EMA-noSV approach for $R_s^{T'}$ deviates significantly from the fully relativistic and projected results, the uncertainty spread (significantly enhanced for the CC1 current) being even larger than that obtained in RPWIA [18]. We should also recall that $R_s^{T'}$ is strongly affected by the choice of the optical potential (results corresponding to the parameterizations EDAIO and EDAD2 are very different from those for EDAD1 and EDAD3). Although not shown in the figure, it is also important to point out that at low q ($q \leqslant 350$ MeV/c), the projection over positive-energies in the bound nucleon wave function clearly dominates, while at higher q, the reverse occurs. This result contrasts with the behavior seen for the unpolarized observables and also with the other three polarized responses, where for high enough transfer momentum projecting out the negative-energy components in the ejected nucleon wave function is proven not to alter the fully relativistic predictions.

The behaviors presented by the four polarized responses, their relative contributions and their sensitivity to dynamical relativistic effects give us important clues to understand the results obtained for the longitudinal and sideways transferred polarization asymmetries. The large effects introduced by relativity in P_l', particularly when comparing full relativistic and projected calculations for CC1, can be traced back to the similar contributions given by the two responses $R_l^{T'}$ and $R_l^{TL'}$ that enter in P_l'. Although relativistic dynamics affect $R_l^{TL'}$ more, their effect on $R_l^{T'}$ is also sizeable. The case of P_s' is clearly different. Here the two polarized responses involved contribute very differently, $R_s^{T'}$ being much smaller (more than one order of magnitude). Therefore, the asymmetry P_s' is almost given uniquely by $R_s^{TL'}$, whose uncertainty due to dynamical relativistic effects presents the lowest spread. Although results for $p_{3/2}$ and $s_{1/2}$ show basically similar behavior to those of the $p_{1/2}$ shell, off-shell and dynamical relativity play a less significant role for the $p_{3/2}$ shell in $R_s^{T'}$ and $R_l^{TL'}$.

As already mentioned, in RDWIA spinor distortion affects both the bound and ejected nucleon wave functions. Hence in what follows, we analyze the role of dynamical relativity, isolating the spinor distortion contribution in each nucleon wave function separately. We show results for the ratios $P'_{l,s}$ and the left-right asymmetry A_{TL}, focusing on the CC2 current, which minimizes dynamical effects, and the $p_{1/2}$ shell. Results for $p_{3/2}$ and $s_{1/2}$ follow the same general trends, but with a significant reduction of the effects due to relativistic dynamics. In Fig. 5 we show the observables for three values of the momentum transfer q. In each case, quasiperpendicular kinematics (q, ω constant) have been selected, and RDWIA and projected calculations are compared. Within the projected results, we distinguish the EMA-noSV approach, where negative-energy components of the bound and scattered nucleon wave functions have been projected out, from the results where the projection over positive-energy components affects only one of the nucleon wave functions: bound (referred to as EMAb) and ejected (EMAf).

From inspection of Fig. 5, a clear difference emerges in the behavior observed for A_{TL} and the polarized ratios $P'_{l,s}$.

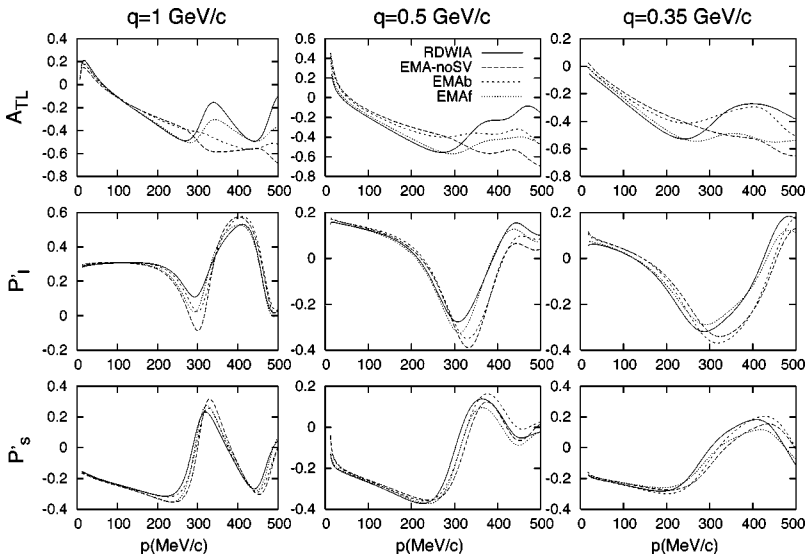

FIG. 5. Left-right asymmetry A_{TL} (top panels) and transferred polarized ratios, P'_l (middle panels) and P'_s (bottom panels) for proton knockout from ^{16}O for the $p_{1/2}$ shell. Results correspond to (q,ω)-constant kinematics with $q=0.35$ GeV/c (right panels), $q=0.5$ GeV/c (middle panels), and $q=1$ GeV/c (left panels). In each case the transfer energy ω is fixed to the quasielastic peak value. RDWIA calculations (solid line) are compared with the EMA-noSV approach (dashed line) and with the results after projecting over positive-energy states for the bound nucleon wave function only (short-dashed line) and for the ejected nucleon only (dotted line).

The asymmetry A_{TL} presents a well established pattern: for low-medium p values the largest effect shows up when projection over positive-energy states in the bound nucleon wave function is assumed (a consequence of the dominance of the direct term in the reaction mechanism for low p). On the contrary, for high p ($p \geqslant 250,300$ MeV/c), the separate influence of each nucleon wave function depends very much on q. At very low q the most sizeable effects correspond to projection of the ejectile wave function state. However, as q increases so does the ejected nucleon momentum p_F; thus FSI effects are expected to be smaller and consequently the contributions of the negative-energy states in the ejected nucleon play a minor role. As noted, the results for $P'_{l,s}$ do not match this general behavior, and it is hard to state which nucleon wave function plays the major role concerning relativistic dynamical effects.

Finally, a basic difference between A_{TL} and $P'_{l,s}$ connects with the oscillatory behavior shown by these observables. While it remains in $P'_{l,s}$ for all q values and all approaches, in the case of A_{TL}, the oscillations disappear when projection is assumed. This effect, connected with factorization breakdown, is analyzed in Ref. [39].

C. Semirelativistic reductions

In this section we focus on the kinematical relativistic effects, i.e., effects associated with the nonrelativistic reduction of the nucleon current operator. In Fig. 6 we present the polarization ratios and *TL* asymmetry for the $p_{1/2}$ shell and same kinematics as in Fig. 1. We compare the RDWIA results (solid line) with the EMA-noSV (dotted line) and semirelativistic approaches. For the latter we distinguish the following: SR (dot-dashed line), corresponding to the expressions in Eqs. (11) and (12), and Nonrel (dashed line) where additional approximations on the vector current have been assumed (see Sec. II C and Refs. [14,31] for details). As shown, the semirelativistic curves follow the shape of the EMA-noSV ones, particularly for A_{TL} where oscillations are largely suppressed within EMA-noSV and semirelativistic approaches. Kinematical effects are observed by comparing EMA-noSV and semirelativistic calculations. As expected, they are very small in the low p region, increasing for high missing momenta. This same general pattern emerges for other transfer momentum values and similar conclusions hold for the $p_{3/2}$ and $s_{1/2}$ shells.

To complete the analysis of kinematical effects we study the individual responses. First, let us consider the unpolarized ones, which are presented in Fig. 7 (top panels) for the $p_{1/2}$ shell and CC2 current operator. The labeling of the curves is as in previous figure. We observe that the pure longitudinal and transverse responses, R^L and R^T, hardly show any dependence on either kinematical or dynamical relativistic effects. This coincides with some previous findings [9,10], but clearly disagrees with the results obtained by Meucci and collaborators [27], who found very different results for R^T using relativistic and nonrelativistic approximations. Concerning R^{TL}, it shows a significant dependence with relativistic nucleon dynamics. This is in accord with our previous analysis [9,28], and also with the results of the Pavia group [27], although in the latter case, the behavior found for R^{TL} within the RDWIA calculation, clearly differs from ours for very low missing momentum. Moreover, note that the difference between EMA-noSV, SR, and Nonrel is negligible. Finally, the response R^{TT} also shows a high sensitivity to both dynamical and kinematical relativistic ingredients, though its smallness makes it difficult to isolate from cross section measurements. Let us also recall that our results do not match those obtained by the Pavia group, particularly for high q values.

Focusing on the transferred polarized responses (bottom panels of Fig. 7), we observe that relativistic ingredients play a very minor role in $R_s^{TL'}$ and $R_l^{T'}$. On the contrary, dynamical relativistic effects are sizeable for $R_l^{TL'}$ and especially for $R_s^{T'}$, while the kinematical relativistic effects are strongly canceled. Note that the EMA-noSV and semirelativistic approaches give rise to almost identical results. Additional restrictions on the nonrelativistic procedure to get the current operator [12–14,31] (Nonrel approach) leads to more visible effects which increase when the transferred energy goes up.

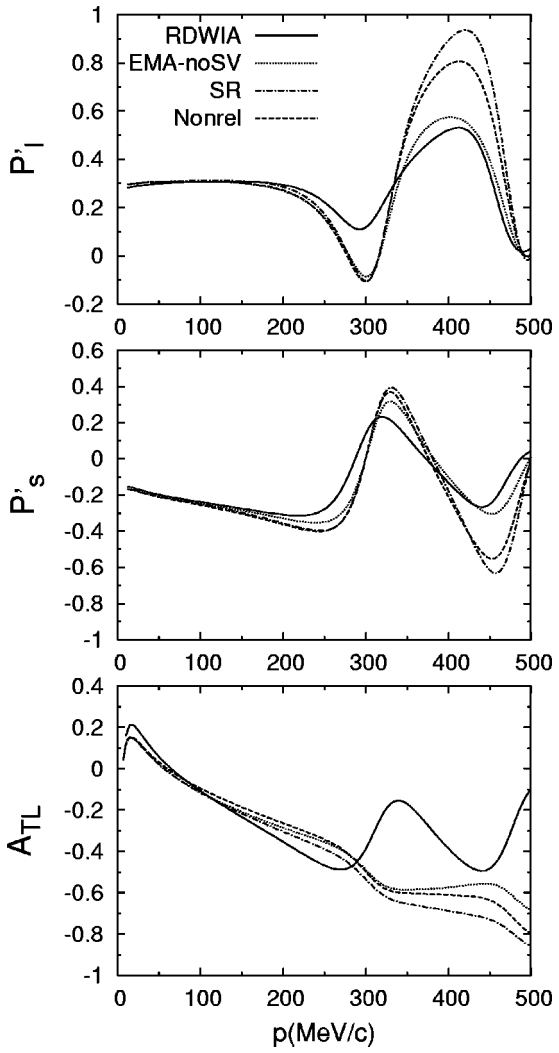

FIG. 6. Transferred polarizations P_l' (top panel) and P_s' (middle panel), and A_{TL} asymmetry (bottom panel) for proton knockout from the $p_{1/2}$ shell in ^{16}O. Results correspond to the RDWIA calculation with the CC2 current operator (solid line), the EMA-noSV approach (dotted line), the semirelativistic current given in Eqs. (11) and (12) (dot-dashed line) and the Nonrel approach (dashed line) (see text for details). All curves have been obtained using the EDAIO optical potential.

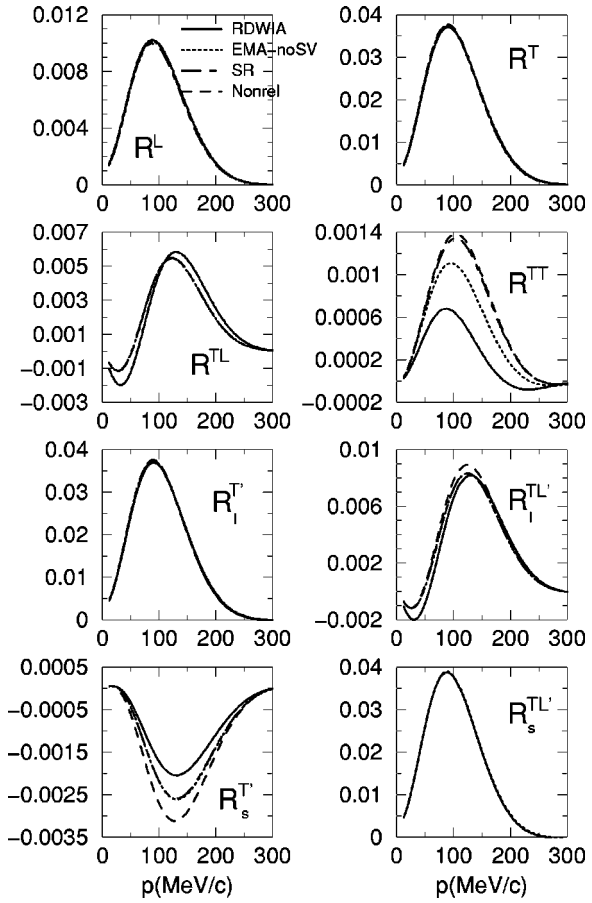

FIG. 7. Unpolarized (top panels) and recoil nucleon polarized (bottom panels) responses for proton knockout from the $p_{1/2}$ shell in ^{16}O. Kinematics as in Fig. 1 and the same labeling as in Fig. 6.

D. Comparison with experimental data

We proceed to compare our calculations with the experimental data recently measured at JLab [1]. The kinematics of the experiment was the same as used in previous figures except that the azimuthal angle was $\phi=180°$ instead of $\phi=0°$. As shown later, this makes an important difference concerning the effects introduced by relativistic dynamics and/or optical potentials. Figure 8 shows P_l' (top panels), P_t' (middle panels), and the ratio P_t'/P_l' (bottom panels) for proton knockout in ^{16}O from the $1p_{1/2}$ (left panels), $1p_{3/2}$ (middle panels) and $1s_{1/2}$ (right panels) shells. Note the change of notation for the transverse polarization transfer observable. In Ref. [1], and only for $\phi=180°$, the vector perpendicular to the plane containing $\mathbf{p}_F$ and the transfer momentum $\mathbf{q}$ is chosen in the opposite direction that we have made in this paper. Consequently there is also a change of sign in the transverse vector. In order to present the experimental data taken in Ref. [1] in the same form as in the original paper, we have preferred to show our curves for P_t' polarization in Fig. 8. P_t' is equal to P_s' for $\phi=0°$ and differs only in a sign with P_s' when $\phi=180°$. Curves corresponding to RDWIA, positive-energy projected and EMA-noSV calculations are presented. The labeling is as in Fig. 3, and all of the results have been obtained using the EDAIO potential.

To make explicit the differences between $\phi=0°$ (kinematics assumed in the previous figures) and $\phi=180°$ (kinematics of the experiment), in each graph we present the polarized observables as functions of the missing momentum, whose range goes from -300 MeV/c to $+300$ MeV/c. Positive p values refer to $\phi=180°$, where the two experimental data are located, and negative ones to $\phi=0°$.

As shown in Fig. 8, all theoretical calculations satisfactorily reproduce the data, improving somehow the general agreement compared with previous semirelativistic analysis [17]. However, it is hard to draw specific conclusions concerning the reliability of the various approaches within this low-p region. For higher p, relativistic dynamics, off-shell effects and FSI start to play an important role. In this sense, from inspection of Fig. 8, it is interesting to point out that choosing $\phi=0°$ clearly enhances dynamical relativistic ef-

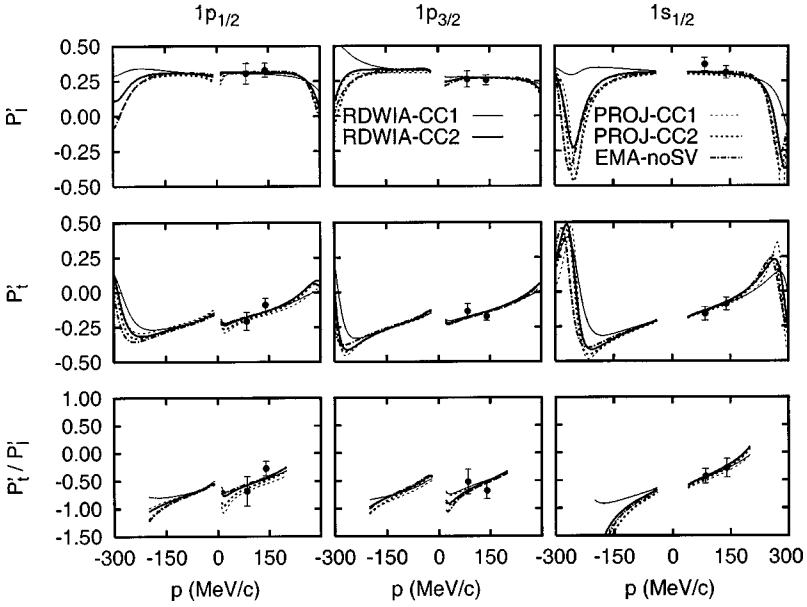

FIG. 8. Transferred polarizations P'_l, P'_t and the ratio P'_t/P'_l compared with experimental data. Positive (negative) p values refer to $\phi = 180°(0°)$. The labeling of the curves is as in Fig. 3. Left, middle, and right panels correspond to $p_{1/2}$, $p_{3/2}$, and $s_{1/2}$ shells, respectively.

fects for P'_l at intermediate p-values, $p \simeq 200-300$ MeV/c. The same comment applies to off-shell and FSI effects. Hence, high quality P'_l data measured for coplanar, $\phi = 0°$ kinematics at intermediate p values can provide precise information to constrain the theoretical models. In the case of P'_t, dynamical uncertainties (also off-shell and FSI effects) are shown to be rather similar for both coplanar $\phi = 0°$ and 180° kinematics.

E. Effects of medium modified form factors

To finish, we present a brief analysis of the effects introduced by possible changes in the nucleon form factors in the nuclear medium. We limit our attention to the same kinematics as in preceding sections. A more exhaustive analysis ranging over different Q^2 values, where the models predict different sensitivity to in-medium effects, will be presented in a forthcoming publication.

The procedure we have used to include these effects in our calculations is as follows. We have taken density-dependent form factors as predicted by the quark-meson coupling model (QMC) [40], computed for a bag radius of 0.8 fm. In order to get well behaved modified form factors in the free case, we have scaled the ones parametrized by Gari and Krumplemann [34] (labeled as GK) with the ratio between the QMC form factors at a given density and those predicted for free conditions,

$$G_{E,M}(Q^2,\rho(\mathbf{r})) = G^{GK}_{E,M}(Q^2)\frac{G^{QMC}_{E,M}(Q^2,\rho(\mathbf{r}))}{G^{QMC}_{E,M}(Q^2,0)}, \qquad (13)$$

where $G^{QMC}_{E,M}(Q^2,\rho(\mathbf{r}))$ are the density-dependent Sachs form factors of the proton immersed in nuclear matter with local baryon density $\rho(\mathbf{r})$. By analogy with the free case, we define density-dependent Dirac and Pauli form factors related to $G_{E,M}(Q^2,\rho(\mathbf{r}))$. Finally, we compute the current matrix elements in coordinate space by introducing these modified

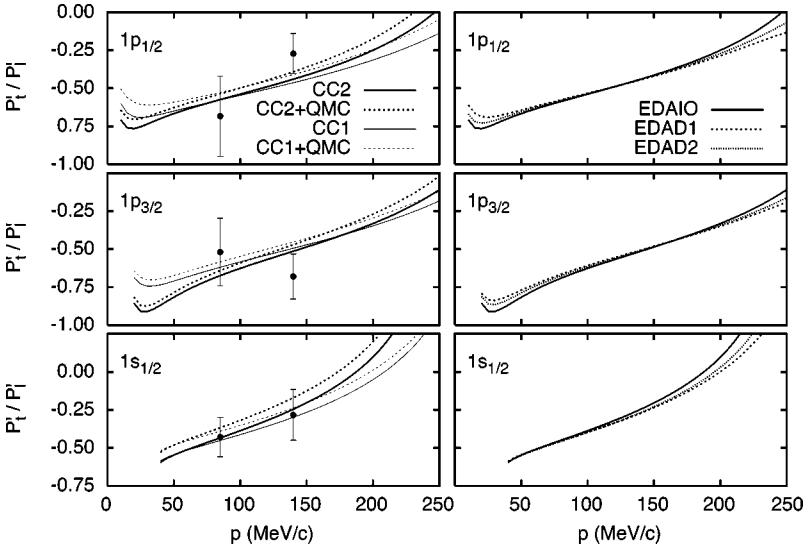

FIG. 9. Effects of medium modified form factors (left panels) and FSI uncertainties (right panels) on the transferred polarization ratio P'_t/P'_l. Results correspond to $\phi = 180°$. Upper, middle, and bottom panels represent the results for $1p_{1/2}$, $1p_{3/2}$, and $1s_{1/2}$, respectively. For the left panels, the free (medium modified) results calculated by using the EDAIO optical potential are represented by solid (dashed) lines. Thick (thin) lines refer to the CC2 (CC1) results, respectively. For the right panels all of the curves have been obtained using CC2. Solid lines correspond to the EDAIO results, dashed lines to EDAD1 and dotted to EDAD2.

form factors into Eqs. (6) and (7), evaluated for the corresponding local density in ^{16}O.

The results obtained for the ratio of transferred polarization asymmetries are presented in Fig. 9 for both current operators. Only the $\phi=180°$ region, where data have been measured, is analyzed. As in the preceding section, we plot P'_t/P'_l instead of P'_s/P'_l. The upper, middle and bottom panels correspond to $1p_{1/2}$, $1p_{3/2}$, and $1s_{1/2}$ knockout, respectively. For completeness, in the right panels of Fig. 9 we also present the uncertainties due to the choice of the optical potential parametrization. As shown, for the p shells our model dependence due to the description of FSI is very small in the region $75 \leqslant p \leqslant 175$ MeV/c ($p \leqslant 100-125$ MeV/c for $1s_{1/2}$), starting to increase for higher p. Within this "safe" region, medium modification effects for the $p_{1/2}$ amount to $\sim 9\%$ ($\sim 7\%$) for the CC1 (CC2) operator at $p \simeq 100$ MeV/c. Note however that even when these effects are sizeable, the uncertainties introduced by the current operator choice can also be noticeable. The situation worsens for the $1p_{3/2}$ shell, for which the free and QMC calculations get mixed due to the off-shell uncertainties. The precision of the actual experimental data [1] does not allow one to state which specific calculation is preferred. However, more precise data, particularly in the region $100 \leqslant p \leqslant 175$ MeV/c for $p_{1/2}$, could help to constrain the theoretical model. In this sense, note that the QMC results differ more clearly from the free calculations in this shell.

For $1s_{1/2}$, the effects of the medium are larger in the vicinity of $p=100$ MeV/c ($\sim 18\%$ for CC2 and $\sim 15\%$ for CC1). Indeed, medium effects are expected to be more important for the inner orbits, due to their higher average densities. The QMC calculations differ substantially from the calculations with free form factors in the p region from 40 to 100 MeV/c, where off-shell ambiguities are very small. In this region it can be possible to disentangle density dependence effects if the error bars of the data are of the order of 10% or less. At larger p values, off-shell ambiguities can make it difficult to contrast our predictions including density-dependence of the form factors versus the free ones, as was the case for the p shells. Moreover, other effects beyond the impulse approximation, not considered in this work, could also play an important role in order to provide a precise description of experimental data for the s shell. We have also computed results with other form factor parametrizations (different from the dipole one), and they change the P'_t/P'_l ratio by about $2-3\%$ for both the free and modified case, keeping the relative differences almost unchanged.

In view of these results we conclude that inferring medium modifications from transfer polarization in ^{16}O at this Q^2 value seems not to be free from ambiguities because of the off-shell effects. However, more precise data and an analysis of other kinematical situations and/or for different nuclei could surely help to draw more definite conclusions.

IV. SUMMARY AND CONCLUSIONS

The analysis of recoil nucleon polarized $(\vec{e},e'\vec{p})$ observables presented in Ref. [18] within RPWIA has been extended here to include FSI described through relativistic optical potentials. The study is restricted to proton knockout from the $p_{1/2}$, $p_{3/2}$, and $s_{1/2}$ shells in ^{16}O and quasiperpendicular kinematics with $q=1$ GeV/c, which roughly corresponds to the experimental setting. A comparison with data is provided.

The main focus of this paper is to study the role played by the dynamical enhancement of the lower components in the bound and scattered nucleon wave functions; along this line, a systematic investigation on the effects linked to FSI and off-shell descriptions is also done. We show results evaluated with the two usual choices of the nucleon current operator, CC1 and CC2, and three different relativistic parameterizations of the optical potential, EDAIO, EDAD1, and EDAD2. Finally, kinematical relativistic effects, associated with the nonrelativistic truncation of the current operator, are also investigated in detail. Additional ingredients, such as the different relativistic models to describe the bound nucleon wave function and nucleon form factors, are seen not to modify our conclusions.

From the results shown in previous sections, we may summarize our basic findings as follows. (i) FSI constitutes a basic ingredient in order to get reliable results to be compared with data. Transferred polarization ratios as well as polarized responses do modify very significantly their structure when FSI are taken into account. However, a kind of cancellation of the FSI effects is observed to occur in P'_l and P'_s for low missing momenta, $p \leqslant 100$ MeV/c. Concerning the role of the optical potential, a clear difference emerges for the two asymmetries at very high p values, $p \geqslant 400$ MeV/c, when comparing results for the EDAIO- and EDAD-type potentials. This is due to the different reduction of the scattered wave function in the nuclear interior produced by the two kinds of optical potentials. Finally, at intermediate p values ($p \simeq 250$ MeV/c), P'_l shows a strong dependence on the interaction model, whereas the uncertainty in P'_s is tinier. A similar comment applies also to the off-shell ambiguities. (ii) Dynamical relativistic effects are shown to be very important, being enhanced for the CC1 current operator. Concerning the responses, $R_s^{T'}$ and $R_l^{TL'}$ present the highest dependence with dynamical effects, as also found in the RPWIA studies. However, contrary to the plane wave limit, where the dynamical enhancement of the lower components of the bound nucleon completely modifies the shape of the transferred asymmetries, in the case of the distorted wave approach the general oscillatory behavior of P'_l and P'_s persists even after projecting out the negative-energy components. This differs also with the behavior of the unpolarized observable A_{TL}. This effect is linked to the breakdown of factorization. At intermediate p-values, P'_l shows a stronger sensitivity to relativistic dynamics. (iii) Results corresponding to semirelativistic reductions are proven to be very similar (depending on the truncation) to the EMA-noSV approach, differing more from the RDWIA calculations. As expected, the difference between the three approaches increases as p goes up. The semirelativistic approaches also lead to a significant cancellation of the oscillatory behavior in A_{TL}, while maintaining the general shape of P'_l and P'_s. This is again connected with the factorization property and its possible breakdown.

From the comparison with experimental data, we show the reliability of our general description of $(\vec{e},e'\vec{p})$ reactions, and conclude that new high quality data measured at intermediate p values (150–200 MeV/c) may help to constrain the various theoretical approximations involved in our calculations.

As pointed out in Ref. [17], other ingredients that go beyond the impulse approximation, such as those arising from meson exchange currents and the Δ-isobar contribution, may also play a very important role in properly describing the transferred polarization asymmetries. These remain to be investigated in a relativistic context, although, in on-going work, the inclusion of two-body currents within the fully relativistic formalism is presently in progress. In the final analysis, any interpretation in terms of medium modified nucleon form factors requires having excellent control of all of these model dependences, both those discussed in the present work and those that go beyond the impulse approximation. Within our model we have found that for the kinematical conditions of E89003 and E89033 [35,36] it is difficult to separate effects introduced by density-dependent form factors from off-shell ambiguities due to the choice of current operator. However, for the $s_{1/2}$ and $p_{1/2}$ shells there is a region in between 40 and 100 MeV/c that is relatively free from off-shell uncertainties and where the effect of medium modifications would be easier to assess. In a future publication we will present the results of a more extensive study in the context of the nuclear model uncertainties and will assess the impact of including medium modifications of the form factors at different values of Q^2.

ACKNOWLEDGMENTS

This work was partially supported by funds provided by DGI (Spain) and FEDER funds, under Contract Nos. BFM2002-03315, BFM2002-03562, FPA2002-04181-C04-04, and BFM2000-0600 and by the Junta de Andalucía (Spain) and in part by the U.S. Department of Energy under Cooperative Research Agreement No. DE-FC02-94ER40818. M.C.M. and J.R.V. acknowledge financial support from the Fundación Cámara (University of Sevilla) and the Consejería de Educación de la Comunidad de Madrid, respectively.

[1] S. Malov *et al.*, Phys. Rev. C **62**, 057302 (2000); S. Malov, PhD thesis, New Brunswick, New Jersey, (1999), unpublished.
[2] S. Dieterich *et al.*, Phys. Lett. B **500**, 47 (2001).
[3] S. Strauch *et al.*, Phys. Rev. Lett. **91**, 052301 (2003).
[4] R. J. Woo *et al.*, Phys. Rev. Lett. **80**, 456 (1998).
[5] J. M. Udías and J. R. Vignote, Phys. Rev. C **62**, 034302 (2000).
[6] J. M Udías, P. Sarriguren, E. Moya de Guerra, E. Garrido, and J. A. Caballero, Phys. Rev. C **48**, 2731 (1993).
[7] J. M Udías, P. Sarriguren, E. Moya de Guerra, E. Garrido, and J. A. Caballero, Phys. Rev. C **51**, 3246 (1995).
[8] J. M. Udías, P. Sarriguren, E. Moya de Guerra, and J. A. Caballero, Phys. Rev. C **53**, R1488 (1996).
[9] J. M. Udías, J. A. Caballero, E. Moya de Guerra, J. E. Amaro, and T. W. Donnelly, Phys. Rev. Lett. **83**, 5451 (1999).
[10] J. M. Udías, J. A. Caballero, E. Moya de Guerra, J. R. Vignote, and A. Escuderos, Phys. Rev. C **64**, 024614 (2001).
[11] J. M. Udías, J. R. Vignote, E. Moya de Guerra, A. Escuderos, and J. A. Caballero, nucl-th/0109077.
[12] J. E. Amaro, J. A. Caballero, T. W. Donnelly, A. M. Lallena, E. Moya de Guerra, and J. M. Udías, Nucl. Phys. **A602**, 263 (1996).
[13] J. E. Amaro, J. A. Caballero, T. W. Donnelly, and E. Moya de Guerra, Nucl. Phys. **A611**, 163 (1996).
[14] J. E. Amaro, M. B. Barbaro, J. A. Caballero, T. W. Donnelly, and A. Molinari, Nucl. Phys. **A643**, 349 (1998).
[15] S. Jeschonnek and T. W. Donnelly, Phys. Rev. C **57**, 2438 (1998).
[16] J. E. Amaro, M. B. Barbaro, J. A. Caballero, and F. Kazemi Tabatabei, Phys. Rev. C **68**, 014604 (2003).
[17] F. Kazemi Tabatabei, J. E. Amaro, and J. A. Caballero, Phys. Rev. C **68**, 034611 (2003).
[18] M. C. Martínez, J. A. Caballero, and T. W. Donnelly, Nucl. Phys. **A707**, 83 (2002).
[19] M. C. Martínez, J. A. Caballero, and T. W. Donnelly, Nucl. Phys. **A707**, 121 (2002).
[20] S. Boffi, C. Giusti, F. D. Pacati, and M. Radici, *Electromagnetic Response of Atomic Nuclei* (Oxford University Press, Oxford, 1996); Phys. Rep. **226**, 1 (1993).
[21] J. J. Kelly, Adv. Nucl. Phys. **23**, 75 (1996).
[22] A. Picklesimer and J. W. Van Orden, Phys. Rev. C **35**, 266 (1987).
[23] A. Picklesimer and J. W. Van Orden, Phys. Rev. C **40**, 290 (1989).
[24] A. S. Raskin and T. W. Donnelly, Ann. Phys. (N.Y.) **191**, 78 (1989).
[25] T. W. Donnelly and A. S. Raskin, Ann. Phys. (N.Y.) **169**, 247 (1986).
[26] T. de Forest, Nucl. Phys. **A392**, 232 (1983).
[27] A. Meucci, C. Giusti, and F. D. Pacati, Phys. Rev. C **64**, 014604 (2001).
[28] J. A. Caballero, T. W. Donnelly, E. Moya de Guerra, and J. M. Udías, Nucl. Phys. **A632** 323 (1998); **A643**, 189 (1998).
[29] B. D. Serot and J. D. Walecka, Adv. Nucl. Phys. **16**, 1 (1986).
[30] J. J. Kelly, Phys. Rev. C **56**, 2672 (1997); **59**, 3256 (1999).
[31] J. E. Amaro, M. B. Barbaro, J. A. Caballero, T. W. Donnelly, and A. Molinari, Phys. Rep. **368**, 317 (2002).
[32] M. M. Sharma, M. A. Nagarajan, and P. Ring, Phys. Lett. B **312**, 377 (1993).
[33] E. D. Cooper, S. Hama, B. C. Clark, and R. L. Mercer, Phys. Rev. C **47**, 297 (1993).
[34] Manfred Gari and W. Krumpelmann, Z. Phys. A **322**, 689 (1985).
[35] W. Bertozzi, K. Fissum, A. Saha, and L. Weinstein (Spokespersons) JLab Experiment E89-003 (unpublished).
[36] C. C. Chang, C. Glashausser, S. Nanda, and P. Rutt (Spokes-

persons) JLab Experiment E89-033 (unpublished).
[37] J. Gao *et al.*, Phys. Rev. Lett. **84**, 3265 (2000).
[38] J. Ryckebusch, D. Debruyne, W. Van Nespen, and S. Janssen, Phys. Rev. C **60**, 034604 (1999); **64**, 044606 (2001).
[39] J. R. Vignote, M. C. Martínez, J. A. Caballero, E. Moya de Guerra, and J. M. Udías, nucl-th/0312076.
[40] D. H. Lu, K. Tsushima, A. W. Thomas, A. G. Williams, and K. Saito, Phys. Lett. B **417**, 217 (1998); Phys. Rev. C **60**, 068201 (1999).